# Control of 4- Switch Three Phase Inverter Fed Induction Motor Drives with Speed and Stator Resistance Estimation at Low and Zero Speed

M. K. Metwally

*Department of electrical Engineering*
*Menoufiya University*
*Menoufiya, Egypt*

mohkamel2007@yahoo.com

***Abstract*— Sensor-less induction motor (IM) drives are widely used in industry for their reliability and flexibility, particularly in hostile environment. However, the performance of many of previously developed observer based speed sensors in very low speeds of IM drives was not satisfactory. In this paper the model reference adaptive system (MRAS) based speed and stator resistance estimators of IM drives fed by four switch three phase inverter (FSTPI) in the critical low and zero speed region of operation is presented. The estimated speed is used as feedback in a vector control system. The MRAS approach has the immediate advantage that model is simple, eliminates the produced error in the speed adaptation, more stable and robust. Simulation results of the MRAS speed observer based sensor-less field-oriented induction motor drives fed by FSTPI are presented at critical low and zero speed region of operations. The performances of the MRAS technique is evaluated in indirect vector control system. Experimental results validate the proposed approach.**

***Keywords: Induction motor, Four switch three phase inverter, Sensor-less control, model reference adaptive system (MRAS).***

## I. INTRODUCTION

Speed controlled induction motor drives are widespread electromechanical systems suitable for a large spectrum of industrial applications. When high dynamic performance and precision control are required for an induction motor in a wide speed range, the speed must be measured. In contrast, in the case of medium and low performance applications, sensorless control without measuring the motor speed is becoming an industrial standard because of advantages in terms of cost, simplicity and mechanical reliability of the drive. As a consequence of this, a great deal of research has been carried out on sensorless drives over the last few decades [1].

Several solutions for sensorless control of induction motor drives have been proposed based on the machine fundamental excitation model and high frequency signal injection methods, as summarized recently [2]. Fundamental model based strategies use the instantaneous values of stator voltages and currents to estimate the flux linkage and the motor speed. Various techniques have been suggested such as, Model Reference Adaptive Systems (MRAS), Luenberger and Kalman-filter observers, sliding-mode observers and Artificial Intelligence (AI) techniques. MRAS schemes offer simpler implementation and require less computational effort compared to other methods and are therefore the most popular strategies used for sensorless control [3, 4].

Various MRAS observers have been introduced in the literature based on rotor flux, back EMF and reactive power [5-8]. However, rotor flux MRAS, first introduced by Schauder [6], is the most popular MRAS strategy and significant attempts have been made to improve its performance [1]. This scheme suffers from parameter sensitivity and pure integration problems [7] which may limit the performance at low and zero speed region of operation [5].

Online adaptation of the stator resistance can improve the performance of the MRAS sensorless drive at low speed [9]. In [4], a simultaneous estimation of rotor speed and stator resistance is presented based on a parallel MRAS observer where both the reference and adaptive models switch roles based on two adaptive mechanisms. Moreover, pure integration for flux represents a crucial difficulty which may cause dc drift and initial condition problems [10, 7, 11].

Low-Pass Filters (LPF) with low cut-off frequency have been proposed to replace the pure integrator [12]. This introduces phase and gain errors and delays the estimated speed relative to the actual, which may affect the dynamic performance of the drive [13, 14] in addition to inaccurate speed estimation below the cut-off frequency [7]. To overcome this problem, Karanayil et al [13] introduce a programmable cascaded low pass filter (PCLPF) to replace the pure integration by small time constant cascaded filters to attenuate the dc offset decay time.

In [15] another technique is used where the rotor flux is estimated by defining a modified integrator having the same frequency response as the pure integrator at steady state. A nonlinear feedback integrator for drift and dc offset compensation has been proposed in [16]. Further research has tried to entirely replace the voltage model (VM) with a state observer with current error feedback or with full order

stator and rotor flux observers which reduces the scheme's simplicity [11, 17].

Semiconductor switches mainly determine the overall price of the power converter devices. So, there has been always a desire to develop new topologies with reduced number of semiconductor devices aiming for reduced costs. Especially in the range of a few ten kilowatts and above, this may cause considerable savings. Among various topologies, half bridge converter has shown the best performance thanks to the reduced number of semiconductor devices, minimized conduction and switching losses, regeneration capability, higher DC link voltage utilization, etc. [18-23].

This converter topology, shown in Fig. 1. a, is often called voltage- doubler. As it can be seen, the DC link voltage is twice the conventional full-bridge converter. This topology is widely employed in industrial applications. The three-phase extension of this topology is shown in Fig. 1.b and is usually referred to as four-switch three phase inverter, component minimized converter, low cost converter or component minimized converter.

This paper presents sensorless control of IM fed by FSTP inverter using MRAS for speed and stator resistance estimation at very low and zero speed operation. Based on the theory of MRAS, simultaneous estimation of rotor speed and stator resistance has been described in this paper. Computer simulations and experimental results are presented to show the effectiveness of proposed approach.

## II. Model of Four Switch Three Phase Inverter

The circuit of Fig. 1.b has two converter legs and third phase is connected to the middle point of the DC link capacitor bank. Because of its benefits, this topology has also found a lot of industrial applications [24,25]. Let us assume that the states of the four power switches are denoted by the binary variables $S_1$ to $S_4$, where the binary "1" corresponds to an ON state and the binary "0" indicates an OFF state. Where $V_s$ is a single phase utility ac supply voltage to dc- voltage, $I_s$ the supply current, and $L_s$ is the boost inductor connected in series with the utility supply voltage.

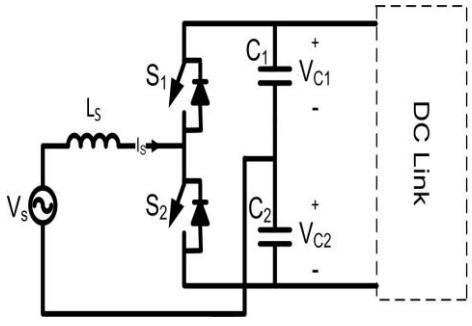


Fig. 1.a: Half-bridge converter (voltage-doubler)

The states of the upper and lower switches in Fig. 1.b of a leg are complementary, which yields:

$$S_3 = 1 - S_1 \quad (1)$$

$$S_4 = 1 - S_2 \quad (2)$$

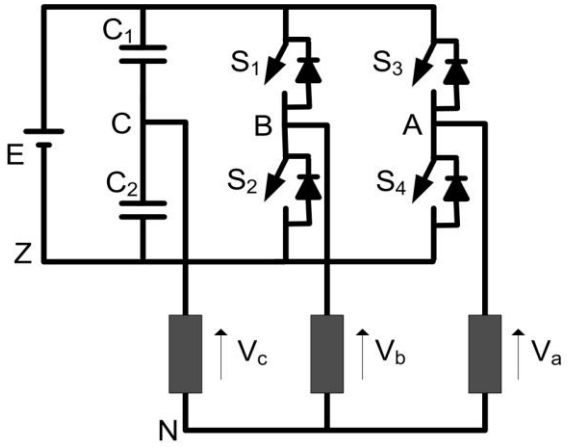


Fig. 1.b: 4-switch voltage source converter.

Let us consider a Y-connection of phases of the induction motor, therefore, their terminal voltages $V_a$, $V_b$ and $V_c$ can be expressed as a function of the states of the upper switches as follows [26].

$$V_a = E(4S_1 - 2S_2 - 1)/6 \quad (3)$$

$$V_b = E(-2S_1 + 4S_2 - 1)/6 \quad (4)$$

$$V_c = E(S_1 + S_2 - 1)/3 \quad (5)$$

Where E is the DC link voltage, Z is the zero voltage point and N is the neutral point. Four combinations of the states of the power switches could be distinguished. These are presented in Table I.

Table I: The four combinations of the states of the power switches and the corresponding terminal voltages $V_a$, $V_b$ and $V_c$

| $S_1$ | $S_2$ | $V_a$ | $V_b$ | $V_c$ |
|---|---|---|---|---|
| 0 | 0 | -E/6 | -E/6 | -E/3 |
| 1 | 0 | E/2 | -E/2 | 0 |
| 1 | 1 | E/6 | E/6 | -E/3 |
| 0 | 1 | -E/2 | E/2 | 0 |

The main drawback of FSTPI is the voltage ripple of DC- link capacitors. To ensure the quality of the output voltages of VSI, we must solve the mentioned above problem by using real time compensation SVPWM technique when generating switching control in consideration of unbalanced DC- link voltages by direct calculation of switching times based on four basic space vectors in FSTP inverter. In [27] the adaptive SVPWM had been used for FSTPI under DC-link voltage ripple condition.

## III. Field Oriented Control Theory

One particular approach for the control of induction motor is the Field Oriented Control (FOC) introduced in [6]. The machine equations in the stator reference frame, written in terms of space vectors, are

$$\bar{U}_s = R_s \bar{I}_s + \frac{d\bar{\psi}_s}{dt} \quad (6)$$

$$0 = R_r \bar{I}_r + \frac{d\bar{\psi}_r}{dt} - j\omega_r \bar{\psi}_r \quad (7)$$

$$\bar{\psi}_s = L_s \bar{I}_s + L_m \bar{I}_r \quad (8)$$

$$\bar{\psi}_r = L_r \bar{I}_r + L_m \bar{I}_r \quad (9)$$

$$\frac{d\omega_r}{dt} = \frac{T - T_L}{J} \quad (10)$$

$$T = P\frac{L_m}{JL_r}(\psi_{rd} i_{sq} - \psi_{rq} i_{sd}) \quad (11)$$

Where, $U_s$, $I_s$, $I_r$ are stator voltage, stator current and rotor current respectively, $R_s$, $R_r$, are the stator and rotor resistances per phase, $L_s$, $L_r$, $\psi_s$, $\psi_r$ are the self inductances and flux of the stator and rotor respectively; $\psi_{rd}$, $\psi_{rq}$, $I_{sd}$, $I_{sq}$ are the rotor flux components in dq-axis and stator current components in dq-axis respectively; $L_m$ is the mutual inductance, $\omega_r$ is the rotor speed, P is the number of poles, T is the electromagnetic developed torque, $T_L$ is the load torque, J is the rotor moment of inertia.

The control strategy is based on the orientation of flux vector along the d-axis which can be expressed by considering.

$$\psi_{rd} = \psi_r \tag{12}$$

$$\psi_{rq} = 0 \tag{13}$$

Assuming a rotor flux reference frame, and developing the previous equations with respect to the d-axis and q-axis components, leads to.

$$\frac{d\psi_{rd}}{dt} + \frac{R_r}{L_r}\psi_{rd} = \frac{L_m R_r}{L_r} i_{sd} \tag{14}$$

$$T = P\frac{L_m}{JL_r}\psi_{rd} i_{sq} \tag{15}$$

## IV. Speed Estimation Scheme Based on MRAS

The speed estimator, analyzed in the paper, is the one originally as in [28] and illustrated in Fig. 2, where the two left-hand side blocks perform integration of equations (16) and (17). It relies on measured stator currents and measured stator voltages and is composed of the reference (voltage) and the adjustable (current) model. The estimator operates in the stationary reference frame (α, β) and it is described with the following equations [28]:

$$p\hat{\underline{\psi}}^s_{rV} = \frac{L_r}{L_m}\left[\underline{u}^s_s - (\hat{R}_s + \sigma L_s p)\underline{i}^s_s\right] \tag{16}$$

$$p\hat{\underline{\psi}}^s_{rI} = \frac{L_m}{T_r}\underline{i}^s_s - \left[\frac{1}{T_r} - j\hat{\omega}\right]\hat{\underline{\psi}}^s_{rI} \tag{17}$$

$$\hat{\omega} = \left[K_{p\omega} + \frac{K_{I\omega}}{p}\right] e_\omega \tag{18}$$

$$e_\omega = \hat{\underline{\psi}}^s_{rI} \times \hat{\underline{\psi}}^s_{rV} = \hat{\underline{\psi}}_{\alpha rI}\hat{\underline{\psi}}_{\beta rV} - \hat{\underline{\psi}}_{\beta rI}\hat{\underline{\psi}}_{\alpha rV} \tag{19}$$

A hat above a symbol in (16)-(19) denotes estimated quantities, symbol *p* stands for *d*/*dt*, *Tr* is the rotor time constant and the leakage coefficient $\sigma = 1 - L_m^2/(L_s L_r)$. All the parameters in the motor and the estimator are assumed to be of the same value, except for the stator resistance (hence a hat above the symbol in (16)). Underlined variables are space vectors, and sub-scripts *V* and *I* stand for the outputs of the voltage (reference) and current (adjustable) models, respectively. Voltage, current and flux are denoted with *u*, *i* and *ψ*, respectively, and subscripts *s* and *r* stand for stator and rotor, respectively. Superscript *s* in space vector symbols denotes the stationary reference frame. As is evident from (16)-(19) and Fig. 2, the adaptive mechanism (PI controller) relies on an error quantity that represents the difference between the instantaneous positions of the two rotor flux estimates. The second degree of freedom, the difference in amplitudes of the two rotor flux estimates, is not utilized. The parallel rotor speed and stator resistance MRAS estimation scheme, which will be developed in the next section, will make use of this second degree of freedom to achieve simultaneous estimation of the two quantities. The role of the reference and the adjustable model will be interchanged for this purpose, since the rotor flux estimate of (17) is independent of stator resistance.

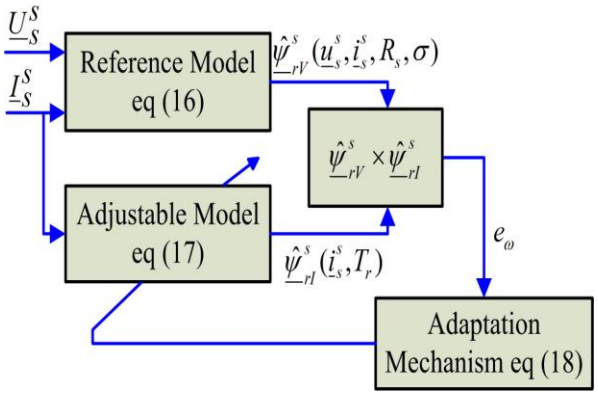


Fig. 2: Basic configuration of the rotor flux based on MRAS speed estimator.

## V. Parallel Rotor Speed and Stator Resistance Estimation

Parallel rotor speed and stator resistance estimation scheme is based on the concept of hyperstability [28] in order to make the system asymptotically stable. For the purpose of deriving an adaptation mechanism it is valid to initially treat rotor speed as a constant parameter, since it changes slowly compared to the change in rotor flux.

The stator resistance of the motor varies with temperature, but variations are slow so that it can be treated as a constant parameter, too. The configuration of the parallel rotor speed and stator resistance is shown in Fig. 3 and is discussed in detail next. Let *Rs* and *ω* denote the true values of the stator resistance of the motor and rotor speed, respectively. These are in general different from the estimated values.

Consequently, a mismatch between the estimated and true rotor flux space vectors appears as well. The error equations for the voltage and the current model outputs can then be written as follows:

$$p\underline{\varepsilon}_V = -\frac{L_r}{L_m}(R_s - \hat{R}_s)\underline{i}^s_s \tag{20a}$$

$$\underline{\varepsilon}_V = \underline{\psi}^s_{rV} - \hat{\underline{\psi}}^s_{rV} = \varepsilon_{\alpha V} + j\varepsilon_{\beta V} \tag{20b}$$

$$p\underline{\varepsilon}_I = \left(j\omega - \frac{1}{T_r}\right)\underline{\varepsilon}_I + j(\omega - \hat{\omega})\hat{\underline{\psi}}^s_{rI} \tag{21a}$$

$$\underline{\varepsilon}_I = \underline{\psi}^s_{rI} - \hat{\underline{\psi}}^s_{rI} = \varepsilon_{\alpha I} + j\varepsilon_{\beta I} \tag{21b}$$

Symbols $\underline{\psi}^s_{rV}$, $\underline{\psi}^s_{rI}$ in (20b), (21b) stand for true values of the two rotor flux space vectors.

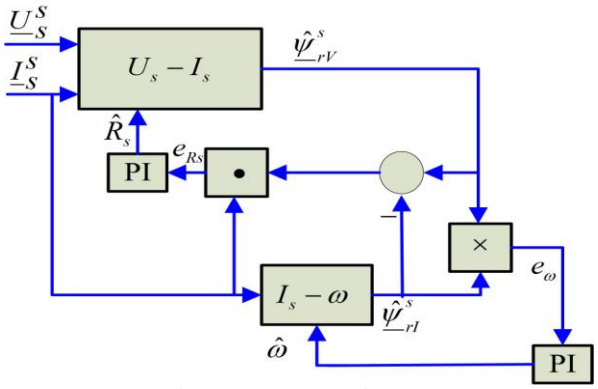


Fig. 3: Structure of the MRAS system of parallel rotor speed and stator resistance estimation.

The system is hyper-stable if the input and output of nonlinear block satisfy Popov's criterion [28]. The adaptive mechanism for rotor speed estimation and stator resistance identification is given in (22), (23) respectively.

$$\hat{\omega} = \left(K_{p\omega} + \frac{k_{I\omega}}{p}\right)\left(\underline{\varepsilon}_I^T . J . \hat{\underline{\psi}}_{rI}^s\right) = \left(K_{p\omega} + \frac{k_{I\omega}}{p}\right) e_\omega \qquad (22)$$

$$J = \begin{bmatrix} 0 & -1 \\ 1 & 0 \end{bmatrix}$$

$$\hat{R}_s = \left(K_{pR_s} + \frac{k_{IR_s}}{p}\right)\left(-\underline{\varepsilon}_V^T . i_s\right) = \left(K_{pR_s} + \frac{k_{IR_s}}{p}\right) e_{R_s} \qquad (23)$$

Where $k_{p\omega}$, $k_{I\omega}$, $k_{pRs,}$ $k_{IRs}$, are PI controller parameters of rotor speed and stator resistance adaptation mechanisms respectively. The role of the reference and the adjustable models is interchangeable in the parallel system of rotor speed and stator resistance estimation. The speed and stator resistance can be estimated in parallel using (22), (23) at any speed. The rotor speed adaptation mechanism (22) is the same as in the customary MRAS speed estimator reviewed in Section IV. Stator resistance adaptation mechanism (23) is, at the first sight, similar to the one of [29,30]. However, stator resistance is here estimated in the stationary reference frame (rather than in the rotor flux oriented reference frame), and error quantity is obtained using two rotor flux space vector estimates (rather than the reference and a single estimated value, as in [30]). Further, stator resistance and rotor speed estimation operate in parallel, rather than sequentially as in [31]. This is enabled by utilizing the second available degree of freedom (the difference in rotor flux amplitudes) in the process of stator resistance estimation.

## VI. Sensorless Speed Control

The overall system of the sensor-less control algorithm is shown in Fig. 4 it incorporates the MRAS system of parallel rotor speed and stator resistance estimation which receive the stator voltages and currents after using low pass filters (LPF). The stator voltage and current are the inputs to voltage model (reference model) the out put is the rotor flux in stationary reference frame. The stator current and estimated rotor speed are the inputs to current model (adaptive model) the output is the rotor flux in stationary reference frame. The error between the two estimated rotor fluxes due to reference model and adaptive model is used to estimate the rotor speed and stator resistance as mentioned before. The estimated speed, reference speed and stator currents as well as reference flux are used as inputs to the field oriented control (FOC) block diagram. The output of FOC is the pulses for FSTP voltage source inverter.

## VII. Simulation and Experimental Results

The machine under test was operated under sensor-less field oriented speed controlled condition. The torque is applied by the load machine under torque controlled mode. The parameters of the machine under test are given in appendix I. The control is done on a digital signal processor board (DSP 1103) plugged into a computer. It performs the vector control algorithm and the hysteresis current controller to generate the pulse sequences for FSTP inverter as shown in Fig. 5.

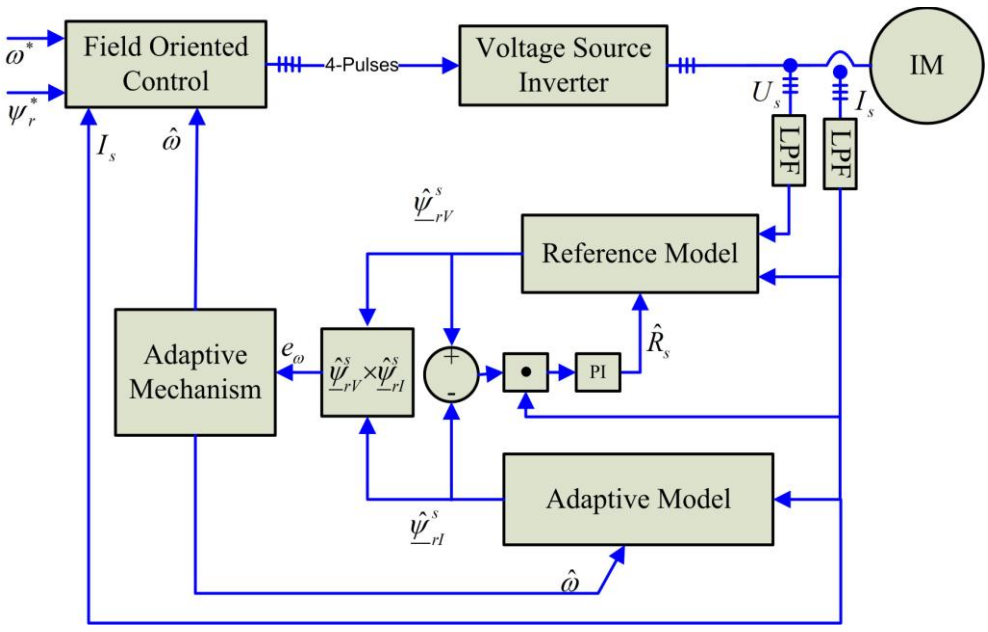


Fig. 4: Configuration of over all sensorless control system

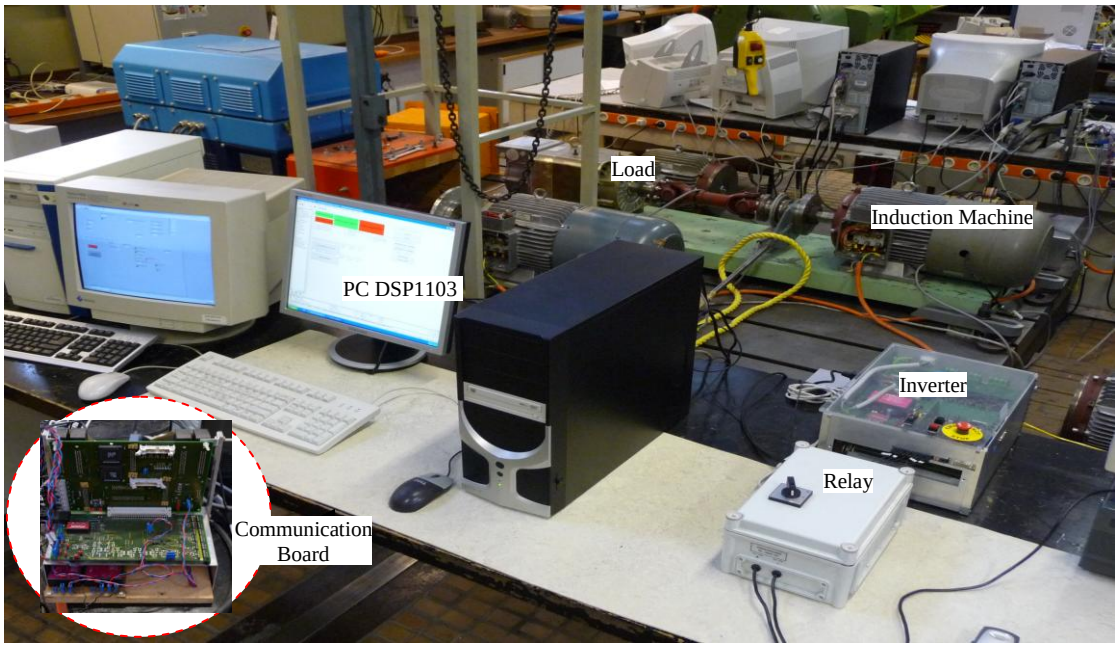


Fig. 5: Experimental setup

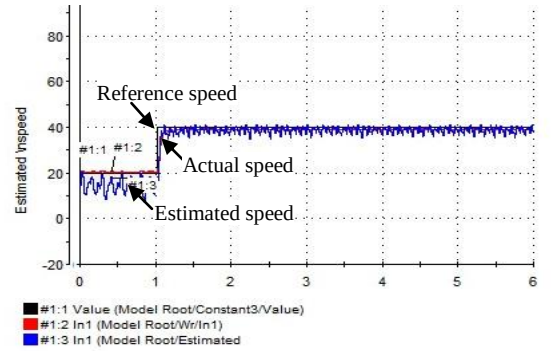


(a)

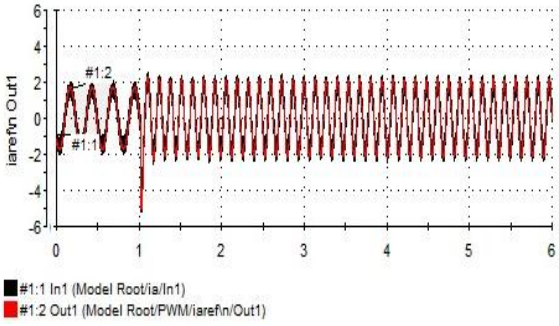


(b)

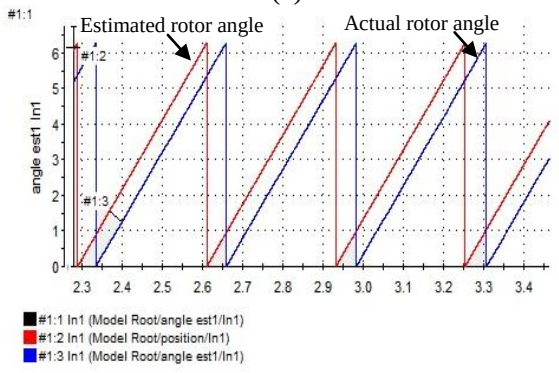


(c)

Fig. 6: Experimental results at speed change from 20 rpm to 40 rpm at time = 1sec (a) motor speed, (b) three phase currents and (c) rotor angles in rad at speed 40 rpm.

There is a communication board for transferring and receiving data between the control algorithm on DSP 1103 and the real time system. The induction motor was fed by a voltage source inverter and two current sensors were used for the current measurements. An optional position signal is available from an encoder with 1024 pulses resolution as a reference signal. The control algorithm is executed by 'simulink', and downloaded to the board through host computer. The outputs of the board are logic signals, which are fed to the three -phase inverter through driver and isolation circuits. The response due to a step change in the speed command is used to evaluate the performance in terms of steady state errors and stability.

Fig. 6.a shows the experimental results of estimate (blue) and actual speed (red) response with a command speed (black) change from 20 rpm to 40 rpm at time = 1 sec at no load.It can be seen that the rotor speed is accelerated smoothly to follow its reference value with nearly zero steady state error. Fig. 6.b shows the motor current of phase (A) and its reference current whereas Fig. 5.c shows the estimated rotor angle (red) and actual rotor angle (blue) in rad. These results show a good correlation between the estimated speed signal and its corresponding actual as well as reference speed signals.

Fig. 7 shows the simulated results of speed waveforms when the sensorless speed control was performed using FSTP inverter at very low and zero speed with load applied at t= 1 sec. The reference speed is changed from 50 rpm at t=3 sec to zero rpm and speed change back from zero rpm to 50 rpm at t=5 sec. The speed command applied in the speed controller is shown Fig. 7 upper diagram (red) in rpm, the estimated speed (blue) and the actual motor speed (black). The load torque is changed from 0 to 80% of rated torque at t=1 sec as shown in Fig. 7 (lower diagram) the speed change and return back to the previous value due to the robust of the control method.

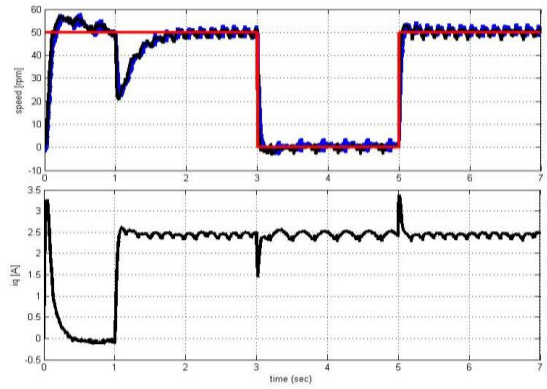


Fig. 7: Upper: Reference speed (red), estimated speed (blue) and actual speed (black) in rpm. Lower: torque current iq (A).

Fig. 8 demonstrates the accuracy of FSTP inverter during load and speed change operations. The upper diagram shows the actual (black) and estimated rotor angles for tests depicted in Fig. 7. The lower diagram shows the same operating state but for the rotor flux angle. The actual (black) and estimated rotor flux angles in degrees. From Fig. 7 and Fig. 8 it can be noted that the tracking of the rotor speed is very accurate using FSTP inverter during transient and steady states operation.

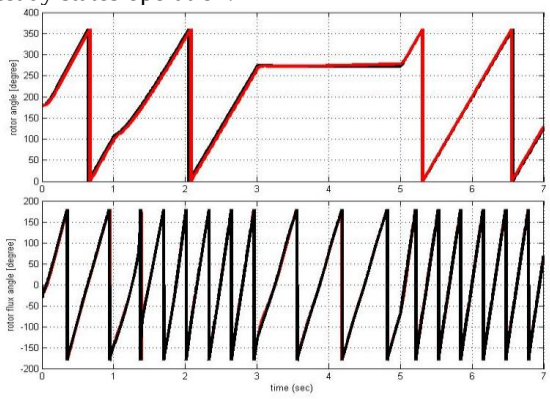


Fig. 8: Upper: Actual rotor angle (black) and estimated rotor angle (red) in °. Lower: Actual rotor flux angle (black) and estimated rotor flux angle (red) in °.

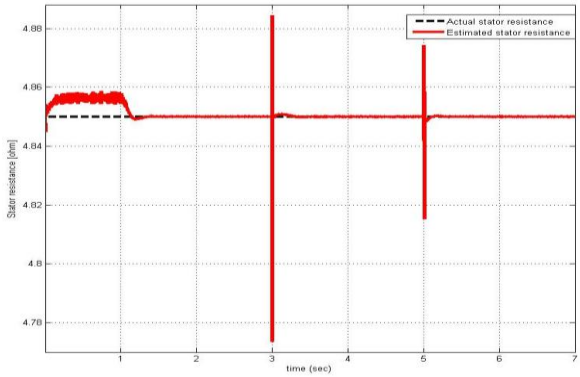


Fig. 9: actual stator resistance (black-dotted) and estimated stator resistance (red) in ohm

Fig. 9 shows the actual (black-dotted) stator resistance and the estimated (red) resistance using the estimation algorithm during the tests depicted in Fig. 7 in ohm the figures show the accuracy of the estimation algorithm during speed and load change operations.

Also Fig. 10 shows the motor current in the stationary reference frame (α,β) (upper diagram) and the three phase motor currents $I_{abc}$ (lower diagram).

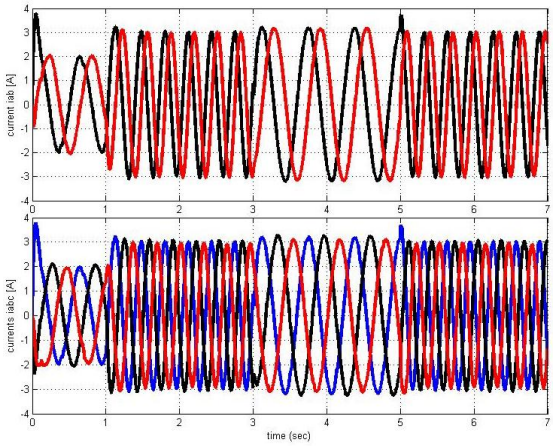


Fig. 10: Upper: motor current in stationary reference frame (αβ) in (A). Lower: motor currents Iabc in (A).

Next, simulated results (Figures. 11-13) are taken when the induction machine speed change ± 50 rpm at load torque 80% is applied at t=1 sec. In the negative speed direction with the slip speed -50 rpm. Since this frequency equals the slip frequency at this load level, the result is zero flux frequency with a constant rotor flux position as shown in fig. 10 (lower diagram). At the time instant of approximately t=5 sec the speed was changed from -50 rpm to 50 rpm. This results in a generating condition of the motor with the flux now rotating in the positive direction. As can be seen, the used technique is able to estimate the flux position that coincides with the reference flux angle during the whole operation, also being stable at zero fundamental frequency.

Fig. 11 (upper diagram) shows the comparison between the reference rotor speed (red) and the sensorless rotor speed with the proposed technique (blue) and the actual rotor speed (black) during speed change ± 50 rpm. The load torque current is shown in Fig. 11 (lower diagram).

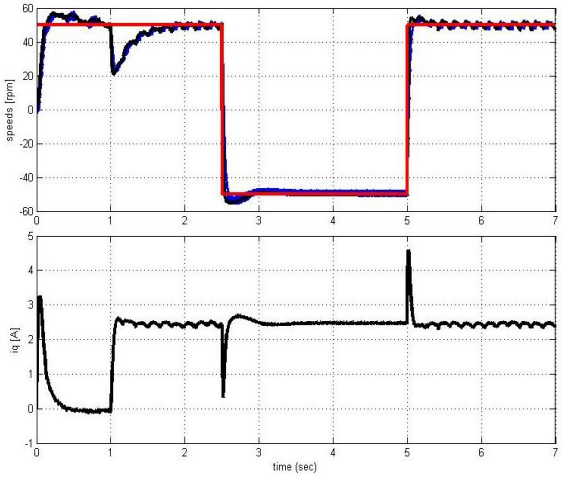


Fig. 11: Upper: Reference speed (red), estimated speed (blue) and actual speed (black) in rpm. Lower: torque current iq (A).

The same comparison is also shown in Fig. 12 (upper diagram) for the estimated rotor angle (red) and actual rotor angle (black). The actual rotor flux angle (black) and the estimated rotor flux angle (red) for the tests depicted in Fig. 11 is shown in Fig. 12 (lower diagram) it is noted that the difference between the actual and estimated rotor angles and rotor flux angles is almost not noticeable as shown in Fig. 12.

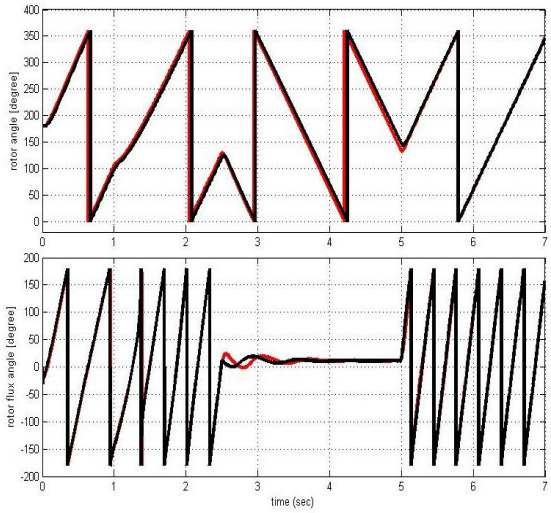


Fig. 12: Upper: Actual rotor angle (black) and estimated rotor angle (red) in °. Lower: Actual rotor flux angle (black) and estimated rotor flux angle (red) in °.

Fig. 13 shows the motor current in the stationary reference frame (α,β) (upper diagram) and the three phase motor currents $I_{abc}$ (lower diagram) for the tests depicted in Fig. 11.

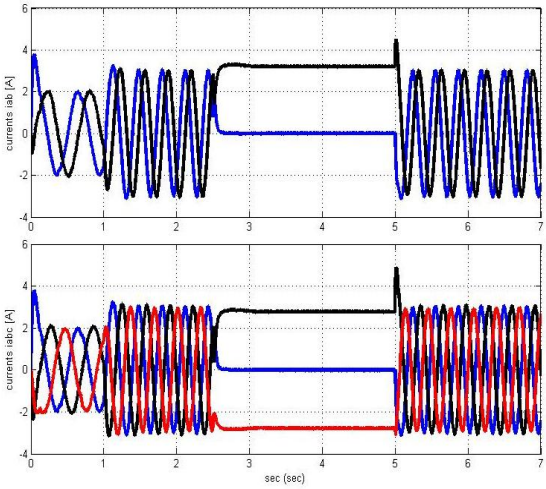


Fig. 13: Upper: motor current in stationary reference frame (αβ) in (A). Lower: motor currents Iabc in (A).

## VIII. Conclusion

The paper presents a new approach for sensorless speed control using FSTPI fed induction motor drives. It is based on MRAS using state observer model with the rotor flux based MRAS technique and the parallel operation of MRAS and stator resistance identification technique comparing to other adaptation technique, this method is simple and needs a low computation power and has a high speed adaptation even at zero speeds. The mathematical description of MRAS using state observer model with the rotor flux is presented also the mathematical description of MRAS in parallel with stator resistance identification is presented.

The proposed method can produce an excellent speed estimation performance in a low speed region and at zero-speed. In addition, the superiority of the proposed method was verified by experimental and simulations in a low and zero speed regions also at zero fundamental frequency operations. Rotor position for a standard induction machine can be tracked reliably under rated flux, high torque levels at low as well as zero speed.

## References


[1] P. Vas, *Sensorless Vector and Direct Torque Control*, Oxford University. Press, 1998.

[2] J. W. Finch and D. Giaouris, "Controlled AC Electrical Drives," *IEEE Transactions on Industrial Electronics*, vol. 55, no. 1, pp. 1-11, February 2008.

[3] M. Rashed and A. F. Stronach, "A stable back-EMF MRAS-based sensorless low speed induction motor drive insensitive to stator resistance variation," *IEE Proceedings Electric Power Applications*, vol. 151, no. 6, pp. 685-693, November 2004.

[4] V. Vasic and S. Vukosavic, "Robust MRAS-Based algorithm for stator resistance and rotor speed identification," *IEEE Power Engineering Review*, vol. 21, no. 11, pp. 39-41, November 2001.

[5] F. Peng and T. Fukao, "Robust speed identification for speed-sensorless vector control of induction motors," *IEEE Transactions on Industry Applications*, vol. 30, no. 5, pp. 1234-1240, September/October 1994.

[6] C. Schauder, "Adaptive speed identification for vector control of induction motors without rotational transducers," *IEEE Transactions on Industry Applications*, vol. 28, no. 5, pp. 1054-1061, September/October 1992.

[7] P. Vas, *Sensorless Vector and Direct torque control.* New York: Oxford University Press, 1998.

[8] S. Maiti, C. Chakraborty, Y. Hori, and M. C. Ta, "Model Reference Adaptive Controller-Based Rotor Resistance and Speed Estimation Techniques for Vector Controlled Induction Motor Drive Utilizing Reactive Power," *IEEE Transactions on Industrial Electronics*, vol. 55, no. 2, pp. 594-601, February 2008.

[9] M. S. Zaky, M. M. Khater, S. S. Shokralla, and H. A. Yasin, "Wide-Speed-Range Estimation With Online Parameter Identification Schemes of Sensorless Induction Motor Drives," *IEEE Transactions on Industrial Electronics*, vol. 56, no. 5, pp. 1699-1707, May 2009.

[10] J. Holtz and J. Quan, "Drift and parameter compensated flux estimator for persistent zero stator frequency operation of sensorless controlled induction motors," *IEEE Transactions on Industry Applications*, vol. 39, no. 4, pp. 1052-1060, July/August 2003.

[11] Y. A. Kwon and D. W. Jin, "A novel MRAS based speed sensorless control of induction motor," in *Proc. the 25th Annual Conference of the IEEE Industrial Electronics Society*, 1999, pp. 933-938.

[12] L. Ben-Brahim, S. Tadakuma, and A. Akdag, "Speed control of induction motor without rotational transducers," *IEEE Transactions on Industry Applications*, vol. 35, no. 4, pp. 844-850, July/August 1999.

[13] B. Karanayil, M. F. Rahman, and C. Grantham, "An implementation of a programmable cascaded low-pass filter for a rotor flux synthesizer for an induction motor drive," *IEEE Transactions on Power Electronics*, vol. 19, no. 2, pp. 257-263, March 2004.

[14] M. Comanescu and L. Xu, "Sliding mode MRAS speed estimators for sensorless vector control of induction machine," *IEEE Transactions on Industrial Electronics*, vol. 53, no. 1, pp. 146-153, February 2006.

[15] M. Hinkkanen and J. Luomi, "Modified integrator for voltage model flux estimation of induction motors," *IEEE Transactions on Industrial Electronics*, vol. 50, no. 4, pp. 818-820, August 2003.

[16] Q. Gao, C. S. Staines, G. M. Asher, and M. Sumner, "Sensorless speed operation of cage induction motor using zero drift feedback integration with MRAS observer," in *Proc. European Conference on Power Electronics and Applications*, 2005.

[17] C. C. Lascu, I. Boldea, and F. Blaabjerg, "A modified direct torque control for induction motor sensorless drive," *IEEE Transactions on Industry Applications*, vol. 36, no. 1, pp. 122-130, 2000.

[18] R. Matinez, and P. N. Enjeti, "A high performance single phase ac to dc rectifier with input power factor correction,"

*IEEE Trans. Power Electron.*, vol. 11, no. 2, pp. 311-317, Mar. 1996.
[19] B. K. Lee, B. Fahimi, and M. Ehsani, "Overview of reduced parts converter topologies for AC motor drives," in *Proc. 2001 IEEE PESC*, pp. 2019-2024.
[20] P.N. Enjeti, and A. Rahman, "A new single-phase to three phase converter with active input current shaping for low cost ac motor drives," *IEEE Trans. Ind. Applicat.*, vol. 29, no. 4, pp. 806-813, July/Aug. 1993.
[21] F. J. C. Padilha, and M. D. Bellar, "Modeling and control of the half-bridge voltage-doubler boost converter," in *Proc. 2003 IEEE ISIE*, pp. 741-745.
[22] R. Madorell, and J. Pou, "Modulation techniques for a low-cost single-phase to three-phase converter," in *Proc. 2004 IEEE ISIE*, pp. 1279-1284.
[23] R. Madorell, J. Pou, J. Zaragoza, P. Rodriquez, and R. Pinado, "Modulation strategies for a low-cost motor drive," in *Proc. 2006 IEEE ISIE*, pp. 1492-1497.
[24] D. O. Neacsu, *Power Switching Converter Medium and High Power*. Florida: CRC, 2006.
[25] Lin, C.-K., Yu, J.-T., Fu, L.-C., Liu, T.-H., and Hsiao, C.-F. "Model-free predictive current controller for four-switch three-phase inverter-fed interior permanent magnet synchronous motor drive systems," in *Proc. 2012 IEEE ASME*, pp. 1048-1053.
[26] Elbadsi, B., Guermazi, A. and Masmoudi, A., "New space vector PWM strategy intended for a low-cost four-switch three-phase inverter-fed induction motor drive", paper presented at CD-ROM of the Third IEEE International Conference on Systems, Signals and Devices, Sousse. (2005).
[27] J. J. Shieh, C. T. Pan, and Z. J. Cuey, "Modeling and design of a reversible three-phase switching mode rectifier," in *Proc. IEE*, vol. 144, no. 6, pp. 389-396, Nov. 1997.
[28] C.Schauder, "Adaptive speed identification for vector control of induction motors without rotational transducers," *IEEE Trans. On Industry Applications*, vol. 28, no. 5, pp. 1054-1061, 1992.
[29] M. Tsuji, S. Chen, K. Izumi, and E. Yamada, "A sensorless vector control system for induction motors using q-axis flux with stator resistance identification," *IEEE Trans. on Industrial Electronics*, vol. 48, no. 1, pp. 185-194, 2001.
[30] K. Akatsu, and A.Kawamura, "Sensorless very low-speed and zero-speed estimations with online rotor resistance estimation of induction motor without signal injection," *IEEE Trans. on Industry Applications*, vol. 36, no. 3, pp. 764-771, 2000.
[31] L. Zhen, and L.Xu, "Sensorless field orientation control of induction machines based on a mutual MRAS scheme," *IEEE Trans. on Industrial Electronics*, vol. 45, no. 5, pp. 824-831, 1998.

## APPENDIX I

The parameters of applied induction machine

| | |
|---|---|
| Rated power | 1 kw |
| Rated load torque | 6.4 N.m. |
| No. of poles | 4 |
| Stator resistance | 4.85 ohm |
| Rotor resistance | 2.6840 ohm |
| Rotor leakage inductance | 0.0221 H |
| Stator leakage inductance | 0.0221 H |
| Mutual inductance | 0.4114 H |
| Supply frequency | 50 Hz |
| Motor speed | 1500 r.p.m. |
| Supply voltage | 380 volts |
| Inertia | 0.018 $kg.m^2$ |